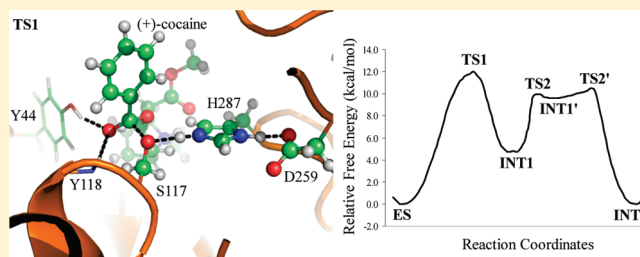


# Reaction Mechanism for Cocaine Esterase-Catalyzed Hydrolyses of (+)- and (-)-Cocaine: Unexpected Common Rate-Determining Step

Junjun Liu,<sup>†</sup> Xinyun Zhao,<sup>†</sup> Wenchao Yang, and Chang-Guo Zhan\*

Department of Pharmaceutical Sciences, College of Pharmacy, University of Kentucky, 789 South Limestone Street, Lexington, Kentucky 40536, United States

**ABSTRACT:** First-principles quantum mechanical/molecular mechanical free energy calculations have been performed to examine the catalytic mechanism for cocaine esterase (CocE)-catalyzed hydrolysis of (+)-cocaine in comparison with CocE-catalyzed hydrolysis of (-)-cocaine. It has been shown that the acylation of (+)-cocaine consists of nucleophilic attack of the hydroxyl group of Ser117 on the carbonyl carbon of (+)-cocaine benzoyl ester and the dissociation of (+)-cocaine benzoyl ester. The first reaction step of deacylation of (+)-cocaine, which is identical to that of (-)-cocaine, is rate-determining, indicating that CocE-catalyzed hydrolyses of (+)- and (-)-cocaine have a common rate-determining step. The computational results predict that the catalytic rate constant of CocE against (+)-cocaine should be the same as that of CocE against (-)-cocaine, in contrast with the remarkable difference between human butyrylcholinesterase-catalyzed hydrolyses of (+)- and (-)-cocaine. The prediction has been confirmed by experimental kinetic analysis on CocE-catalyzed hydrolysis of (+)-cocaine in comparison with CocE-catalyzed hydrolysis of (-)-cocaine. The determined common rate-determining step indicates that rational design of a high-activity mutant of CocE should be focused on the first reaction step of the deacylation. Furthermore, the obtained mechanistic insights into the detailed differences in the acylation between the (+)- and (-)-cocaine hydrolyses provide indirect clues for rational design of amino acid mutations that could more favorably stabilize the rate-determining transition state in the deacylation and, thus, improve the catalytic activity of CocE. This study provides a valuable mechanistic base for rational design of an improved esterase for therapeutic treatment of cocaine abuse.



## INTRODUCTION

Cocaine is recognized as the most reinforcing drug of abuse.<sup>1–3</sup> Recent surveys in the United States show that, among the causes of illicit-drug-related emergency department visits, cocaine is the first on the list.<sup>4,5</sup> Disastrous medical and social consequences of cocaine addiction have made the development of an anticocaine medication a high priority.<sup>6,7</sup> There is still no FDA-approved medication for treatment of cocaine abuse and toxicity.<sup>8–12</sup>

Cocaine esterase (CocE)<sup>13</sup> is the most efficient native enzyme for metabolizing the naturally occurring cocaine yet identified.<sup>14</sup> In rodent models, CocE can both prevent and reverse extreme cocaine toxicity<sup>15,16</sup> and even robustly protects rodents from the lethal effects of cocaine.<sup>17</sup> Although native CocE is unstable at physiological temperature, CocE mutants designed by a novel computational approach significantly improved its thermostability, increasing the probability of clinical application of this enzyme for therapeutic use against cocaine.<sup>18–21</sup>

Cocaine has two enantiomers: one is the naturally occurring (-)-cocaine, which is biologically active; the other is synthetic and biologically inactive (+)-cocaine. A remarkable difference between (-)- and (+)-cocaine is associated with the relative positions of the methyl ester group (Chart 1). The methyl ester group of (-)-cocaine remains on the same side of the carbonyl of the benzoyl ester, whereas the methyl ester group of (+)-cocaine

remains on the opposite side. The structural difference could cause a difference in hydrogen bonding, electrostatic, and van der Waals interactions during the catalytic process and result in a significant difference in free energies of activation. Understanding such a mechanistic difference has been proven beneficial to computational design of high-activity mutants of human butyrylcholinesterase (BChE) against (-)-cocaine.<sup>9,22–27</sup> In particular, the catalytic efficiency of native human BChE against (-)-cocaine is 3 orders of magnitude lower than that against (+)-cocaine.<sup>23</sup> With an effort to understand the mechanistic differences between the BChE-catalyzed hydrolyses of (+)- and (-)-cocaine, our further computational design followed by wet experimental studies<sup>23,24,27–31</sup> has resulted in discovery of various BChE mutants with a considerably improved catalytic efficiency against (-)-cocaine.<sup>9,11,12,24,29–31</sup> One of the BChE mutants has a ~2000-fold improved catalytic efficiency against (-)-cocaine compared to wild-type BChE.<sup>11</sup>

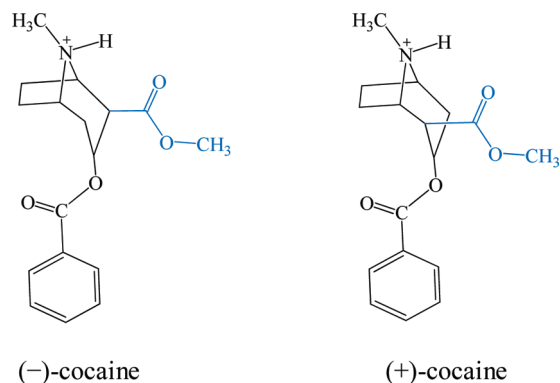
On the basis of the background discussed above, it is important to understand the mechanistic differences between the CocE-catalyzed hydrolyses of (+)- and (-)-cocaine, as their

Received: January 29, 2011

Revised: March 22, 2011

Published: April 12, 2011

Chart 1. Structures of (–)-Cocaine and (+)-Cocaine



mechanistic differences could be beneficial to the design of high-activity mutants of CocE against cocaine. In a previous study,<sup>32</sup> we have elucidated the catalytic mechanism of CocE-catalyzed hydrolysis of (–)-cocaine. However, the detailed catalytic mechanism of CocE-catalyzed hydrolysis of (+)-cocaine remains unknown. To understand the mechanistic differences between the (+)- and (–)-cocaine hydrolyses, it is also necessary to uncover and understand the reaction mechanism of CocE-catalyzed (+)-cocaine hydrolysis. For this purpose, the present study was first focused on the detailed mechanism of CocE-catalyzed hydrolysis of (+)-cocaine.

X-ray crystallographic<sup>14</sup> and site-directed mutagenesis<sup>33</sup> studies have revealed that CocE is a serine carboxylesterase with a catalytic triad formed by Ser117, His287, and Asp259 and with an oxyanion hole formed by the backbone amide of Tyr118 and the hydroxyl group of Tyr44. In light of the mechanistic insights obtained from our recent computational studies on CocE-catalyzed hydrolysis of (–)-cocaine as well as BChE-catalyzed hydrolysis of carboxylic esters (e.g., acetylcholine, butyrylcholine, (+)-cocaine, and (–)-cocaine),<sup>11,12,22,26,27,34–36</sup> CocE-catalyzed hydrolysis of (+)-cocaine might undergo a pathway similar to that for CocE-catalyzed hydrolysis of (–)-cocaine consisting of two major stages. The first stage is acylation, leading to formation of a covalent bond between (+)-cocaine and the enzyme and the departure of ecgonine methyl ester of (+)-cocaine. The second stage is deacylation, resulting in the dissociation of the (+)-cocaine benzoyl ester and enzyme, in which a water molecule acts as the nucleophile and the free form of enzyme is restored.

Notably, the (–)- and (+)-cocaine hydrolyses share the same deacylation stage (see Scheme 1), and thus, in the present study, we first focused on the reaction coordinate calculations on the first stage, i.e., acylation, of CocE-catalyzed hydrolysis of (+)-cocaine. The pseudobond first-principles quantum mechanical/molecular mechanical free energy (QM/MM-FE) approach,<sup>37–40</sup> which has been demonstrated to be a powerful tool in simulating a variety of enzymes,<sup>11,32,41–52</sup> was employed to uncover the detailed reaction pathway and determine the free energy profile for CocE-catalyzed hydrolysis of (+)-cocaine. The computational simulations were followed by wet experimental tests. The computational data demonstrate that the rate-determining step for CocE-catalyzed hydrolysis of (+)-cocaine should be the same as that for CocE-catalyzed hydrolysis of (–)-cocaine, unlike the reported findings for BChE-catalyzed hydrolyses of (+)-cocaine and (–)-cocaine. The new insights into the catalytic mechanisms of CocE against (+)- and (–)-cocaine have been supported by wet experimental kinetic data.

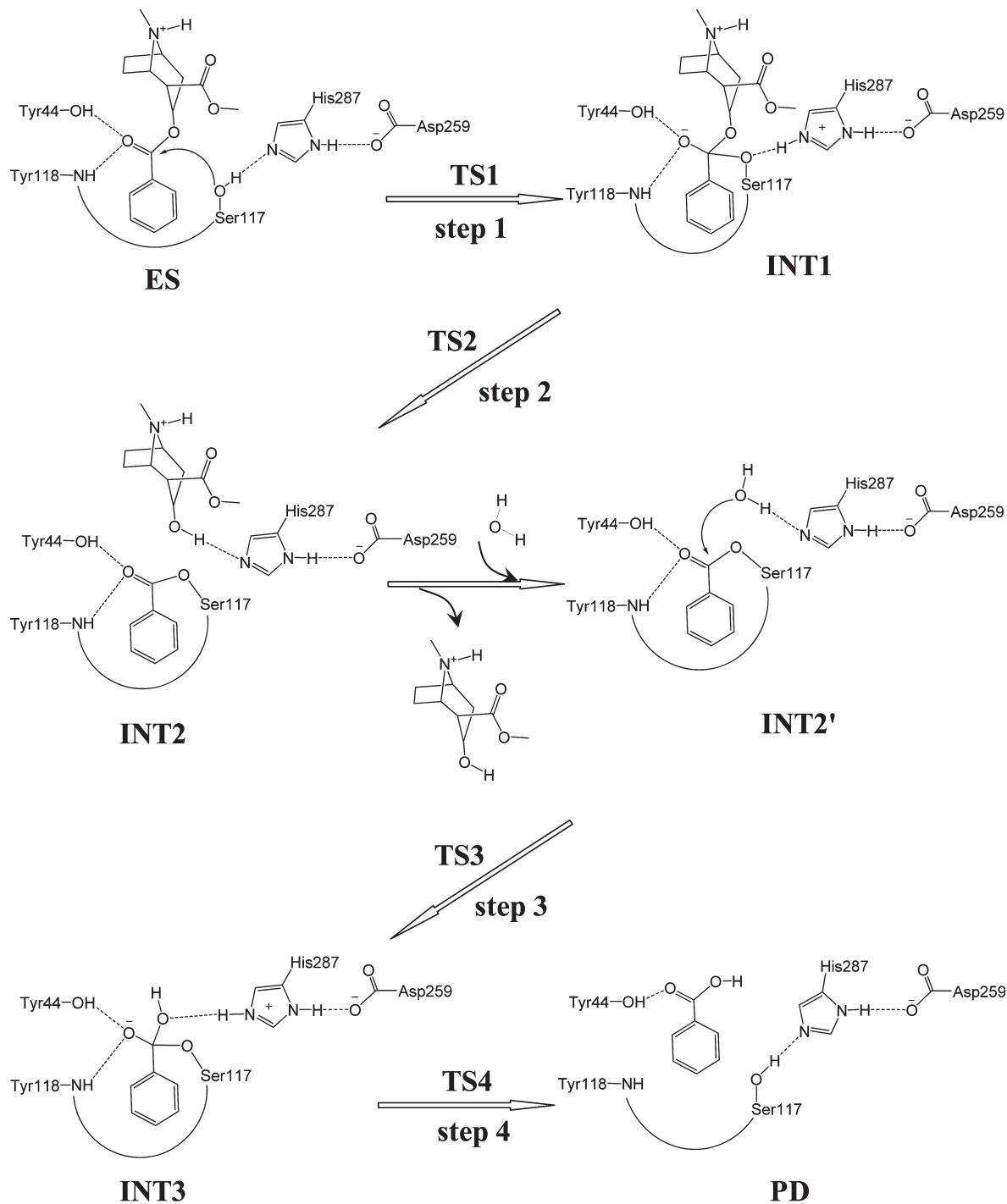
## COMPUTATIONAL AND EXPERIMENTAL METHODS

**QM/MM-FE Simulation.** All of the QM/MM calculations were performed by a pseudobond QM/MM method<sup>37,38</sup> implemented recently in a revised version<sup>11</sup> of the Gaussian 03 and AMBER 8 programs. The QM–MM interface was treated by a pseudobond approach, where a seven-valence-electron atom with an effective core potential is constructed to replace the boundary atom of the environment part and to form a pseudobond with the boundary atom of the active part. The starting structure of the CocE–(+)-cocaine complex was constructed by using the same strategy as used in our previous study on the fundamental mechanism of CocE-catalyzed hydrolysis of (–)-cocaine.<sup>32</sup> The coordinates of CocE from the previously QM/MM-optimized structure of prereactive CocE–(–)-cocaine complex and the structure of (+)-cocaine were used in the molecular docking simulation followed by a  $\sim 4$  ns MD simulation to understand the detailed binding mode of CocE binding with (+)-cocaine. In QM/MM calculations, all atoms of (+)-cocaine and the side chains of Ser117, His287, and Asp259 were considered as the QM atoms, whereas the other atoms were regarded as MM atoms (Figure 1). The QM/MM calculations were performed using an iterative minimization procedure<sup>39</sup> at the B3LYP/6-31G\*:AMBER level; i.e., the QM calculations were carried out at the B3LYP/6-31G\* level, whereas the MM calculations were carried out by using the AMBER force field implemented in the AMBER 8 program.<sup>53</sup> For the QM subsystem, the convergence criterion for geometry optimizations follows the original Gaussian 03<sup>54</sup> defaults; for the MM subsystem, the geometry optimization convergence criterion is the root-mean-square deviation (rmsd) of the energy gradient less than  $0.1 \text{ kcal} \cdot \text{mol}^{-1} \cdot \text{\AA}^{-1}$ . An iterative restrained optimization procedure<sup>39</sup> was then repeatedly applied to different points along the reaction coordinate, resulting in a minimum-energy path. Full QM/MM geometry optimizations at the B3LYP/6-31G\*:AMBER level followed by vibrational frequency analyses were performed to characterize the reactant, intermediates, and transition states. The contribution of the QM subsystem fluctuation to the free energy change was then calculated with the obtained vibrational frequencies using the harmonic approximation. In addition, single-point energy calculations were carried out at the QM/MM(MP2/6-31+G\*:AMBER) level for each geometry along the minimum-energy path.

The free energy changes associated with the QM–MM interaction were then determined by the free energy perturbation (FEP) method<sup>39,40</sup> using a revised version<sup>32</sup> of the AMBER 8 program. The FEP calculations enabled us to more reasonably determine relative free energy changes due to the QM–MM interaction. In the FEP calculations, sampling of the MM subsystem was carried out with the QM subsystem frozen at different states along the reaction path.<sup>39</sup> Technically, the final (relative) free energy determined by the QM/MM-FE calculations is the QM part of the QM/MM energy (excluding the Coulombic interaction energy between the point charges of the MM atoms and the electrostatic potential (ESP) charges of the QM atoms) plus the relative free energy change determined by the FEP calculations. In FEP calculations, the time step used was 2 fs, and bond lengths involving hydrogen atoms were constrained. In sampling of the MM subsystem by MD simulations, the temperature was maintained at 298.15 K. Each FEP calculation consisted of 50 ps of equilibration and 300 ps of sampling.

The MD simulations and QM/MM-FE calculations were performed on a supercomputer (e.g., IBM X-series cluster with

Scheme 1. Proposed Catalytic Mechanism for CocE-Catalyzed Hydrolysis of (+)-Cocaine



340 nodes or 1360 processors) at the University of Kentucky Center for Computational Sciences. The other less-time-consuming modeling and computations were carried out on SGI Fuel workstations and a 34-processor IBM x335 Linux cluster in our own laboratory.

**Expression and Purification of Cocaine Esterase.** A potential problem in wet experimental studies on CocE was that the wild-type enzyme is unstable, with a half-life of only  $\sim 10$  min at  $37^\circ\text{C}$ . Due to the low thermostability, it was difficult to accurately measure the catalytic activity in wet experiments.

Nevertheless, a thermostable version of CocE (i.e., the T172R/G173Q mutant) was developed recently.<sup>18</sup> The T172R/G173Q mutations significantly increase the half-life of CocE to  $\sim 5\text{--}6$  h at  $37^\circ\text{C}$  without changing its catalytic function because residues 172 and 173 are not in the active site. Therefore, to accurately measure the kinetic parameters of the enzyme, we carried out the kinetic characterization using the thermostable version of CocE. The previously prepared CocE cDNA cloned in a bacterial expression vector, pET-22b(+),<sup>18</sup> was used to express the enzyme as 6His-tagged proteins in *Escherichia coli* BL-21

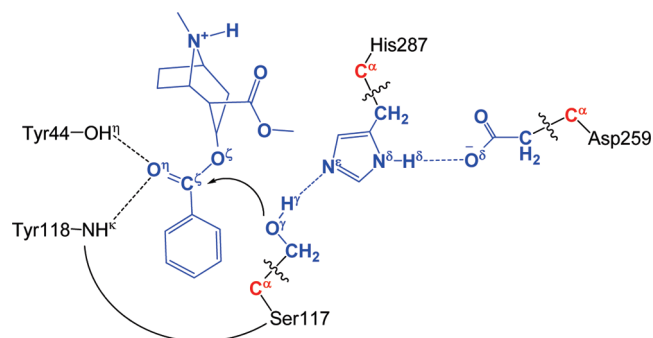


**Figure 1.** Division of the QM/MM system for simulating the acylation stage of CocE-catalyzed hydrolysis of (+)-cocaine. Atoms in blue are treated by the QM method. Three boundary carbon atoms ( $C^{\alpha}$ , colored in red) are treated with the improved pseudobond parameters.<sup>37</sup> All other atoms belong to the MM subsystem.

(DE3) cells grown at 37 °C. Protein expression was induced with 1 mM isopropyl  $\beta$ -thiogalactopyranoside (Sigma-Aldrich) for ~15 h at 18 °C. Cells were pelleted, resuspended in 50 mM Tris-HCl, pH 8.0, 150 mM NaCl, and a protease inhibitor cocktail (34  $\mu$ g/mL concentration each of L-tosylamido-2-phenylethyl chloromethyl ketone, 1-chloro-3-tosylamido-7-amino-2-heptanone, and phenylmethanesulfonyl fluoride and 3  $\mu$ g/mL concentration each of leupeptin and lima bean trypsin inhibitor), and lysed using a French press (Thermo Fisher Scientific, Waltham, MA). The 6His-tagged enzyme was enriched using HisPur cobalt resin (Thermo Fisher Scientific) storage buffers containing 20 mM HEPES, pH 8.0, 2 mM  $MgCl_2$ , 1 mM EDTA, and 1 mM dithiothreitol. The fractions were concentrated by using an Amicon Ultra-50K centrifuge (Millipore, Billerica, MA). The enzyme concentration was determined using a CB-Protein Assay kit (from CALBIOCHEM) with bovine serum albumin as a standard.

**Michaelis–Menten Kinetics of Cocaine Esterase.** The catalytic activities of the enzyme against (+)- and (–)-cocaine were determined at the same time under the same experimental conditions. The initial rates of the enzymatic hydrolysis of (+)/(–)-cocaine were estimated by following the change in the intrinsic absorbance of (+)/(–)-cocaine at 230 nm with time using a GENios Pro microplate reader (TECAN, Research Triangle Park, NC) with the XFluor software. The initial rates were estimated from the linear portion of the progress curves and spanned no longer than 15 min. The reaction was initiated by adding 100  $\mu$ L of an enzyme solution (phosphate-buffered saline (PBS; pH 7.4) to 100  $\mu$ L of a cocaine solution (50 ng/mL enzyme, 100 mM phosphate buffer, pH 7.4). Final (+)/(–)-cocaine concentrations were as follows: 100, 50, 20, 15, 10, 7.5, 5, and 2.5  $\mu$ M.  $V_{max}$  and  $K_M$  values were calculated by using Prism 5 (GraphPad Software Inc., San Diego, CA). All of the activity assays were performed at room temperature (~25 °C).

## RESULTS AND DISCUSSION

**Reaction Pathway.** Our QM/MM reaction coordinate calculations at the B3LYP/6-31G\*:AMBER level revealed that the acylation stage of CocE-catalyzed (+)-cocaine hydrolysis reaction consists of two reaction steps. The first reaction step is the nucleophilic attack on the carbonyl carbon ( $C^{\zeta}$ ) of (+)-cocaine benzoyl ester by the  $O^{\gamma}$  atom in the Ser117 site chain. The second reaction step is the dissociation between the benzoyl ester

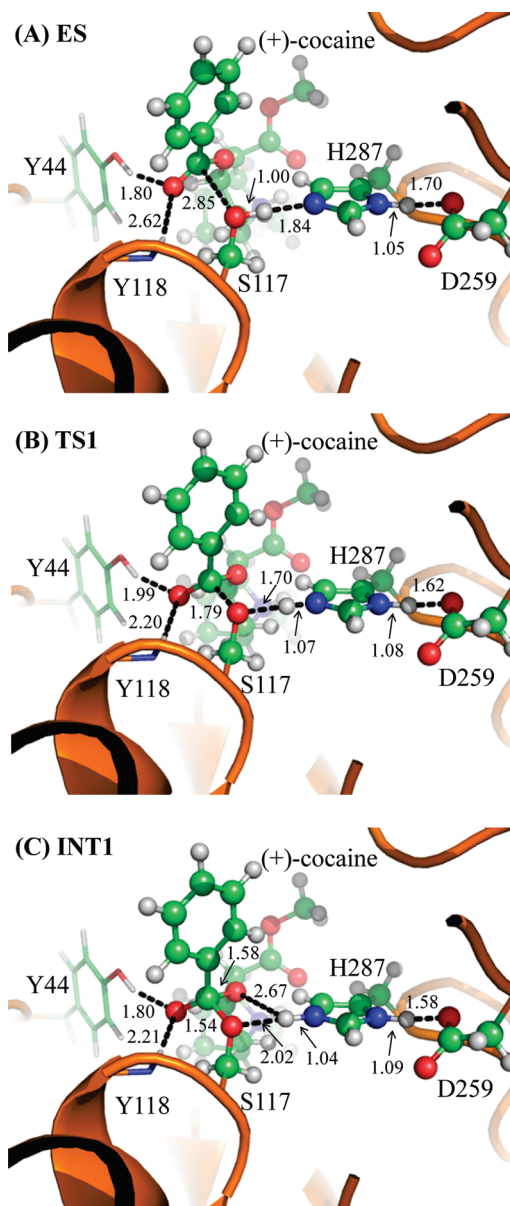


**Figure 2.** Key configurations for reaction step 1, the nucleophilic attack by the  $O^{\gamma}$  atom of Ser117. The geometries were optimized at the QM/MM(B3LYP/6-31G\*:AMBER) level. The key distances in the figure are in angstroms. Carbon, oxygen, nitrogen, and hydrogen atoms are colored in green, red, blue, and white, respectively. The backbone of the protein is rendered as a cartoon and colored in orange. The QM atoms are represented as balls and sticks and the surrounding residues rendered as sticks. The configurations in Figure 3 are represented using the same method.

and ecgonine methyl ester of (+)-cocaine. The optimized geometries of the reactant, intermediates, and transition states are shown in Figures 2 and 3. Below we discuss each of these reaction steps in detail.

During the first step of the catalytic reaction, the nucleophilic attack process proceeds as the serine hydroxyl oxygen, i.e.,  $O^{\gamma}$  atom of Ser117, gradually approaches the  $C^{\zeta}$  atom of (+)-cocaine benzoyl ester. Meanwhile, the serine hydroxyl hydrogen, i.e.,  $H^{\gamma}$  atom of Ser117, gradually moves toward the nitrogen ( $N^{\epsilon}$ ) atom of the His287 side chain. Since this reaction step involves the breaking of the  $O^{\gamma}$ - $H^{\gamma}$  bond and formation of both  $C^{\zeta}$ - $O^{\gamma}$  and  $N^{\epsilon}$ - $H^{\gamma}$

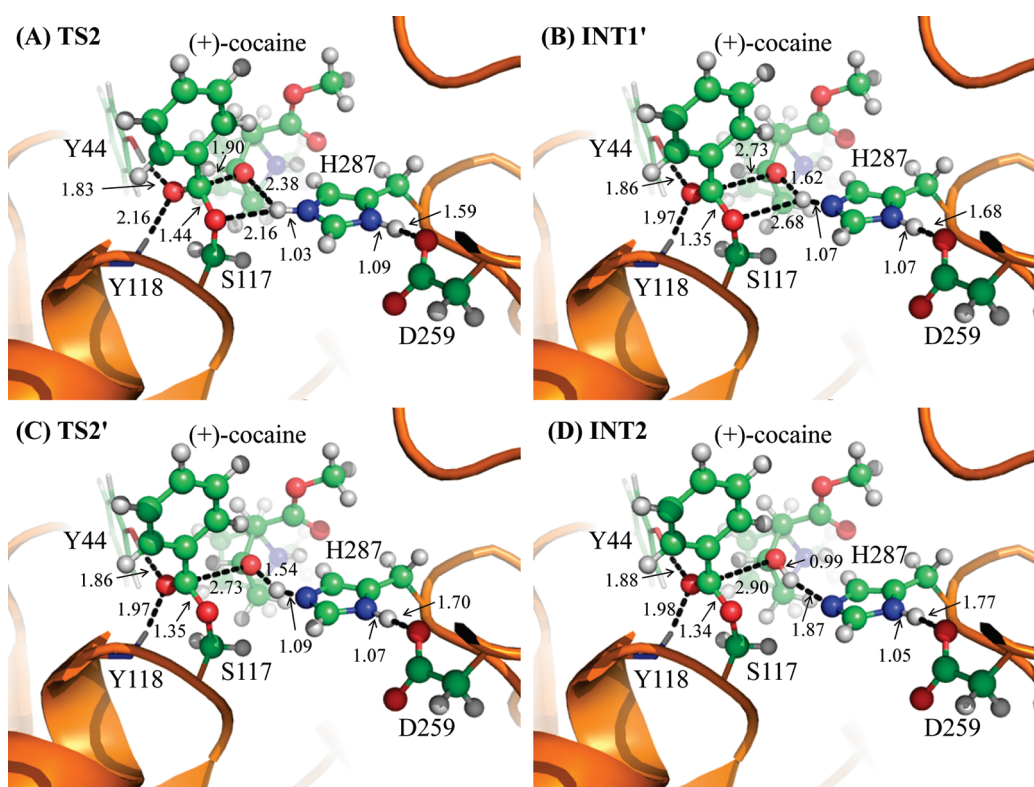


**Figure 3.** Key configurations except INT1 for reaction step 2, the dissociation of (+)-cocaine benzoyl ester. The geometries were optimized at the QM/MM(B3LYP/6-31G\*:AMBER) level. The structure of INT1 is given in Figure 2C.

bonds as shown in Scheme 1, the distances between  $O^{\gamma}$  and  $H^{\gamma}$  ( $R_{O^{\gamma}-H^{\gamma}}$ ), between  $C^{\zeta}$  and  $O^{\gamma}$  ( $R_{C^{\zeta}-O^{\gamma}}$ ), and between  $N^{\epsilon}$  and  $H^{\gamma}$  ( $R_{N^{\epsilon}-H^{\gamma}}$ ) reflect the nature of the first chemical reaction step. Therefore, the reaction coordinate for the first reaction step was set as  $R_{O^{\gamma}-H^{\gamma}} - R_{C^{\zeta}-O^{\gamma}} - R_{N^{\epsilon}-H^{\gamma}}$ . As shown in the QM/MM-optimized geometries (Figure 2), as the  $O^{\gamma}$  atom of Ser117 gradually approaches the  $C^{\zeta}$  atom, the geometry of the reactant (ES), in which the  $C^{\zeta}$  atom is  $sp^2$  hybridized and is in a planar geometry with its three bonding atoms, gradually changes into a tetrahedral geometry centered on the  $sp^3$ -hybridized  $C^{\zeta}$  atom in an intermediate (INT1) through a transition state (TS1).

During the dissociation of (+)-cocaine benzoyl ester, the ecgonine group of (+)-cocaine gradually departs from the (+)-cocaine benzoyl ester group in which the benzoyl ester bond  $C^{\zeta}-O^{\zeta}$  is broken. Meanwhile, the proton ( $H^{\gamma}$ ) attached to the  $N^{\epsilon}$  atom of the His287 side chain transfers to the benzoyl ester oxygen atom ( $O^{\zeta}$ ) of (+)-cocaine. The changes of the distances  $R_{C^{\zeta}-O^{\zeta}}$ ,  $R_{O^{\zeta}-H^{\gamma}}$ , and  $R_{N^{\epsilon}-H^{\gamma}}$  reflect the nature of a dissociation process. Thus, the reaction coordinate for the second reaction step was chosen as  $R_{C^{\zeta}-O^{\zeta}} + R_{N^{\epsilon}-H^{\gamma}} - R_{O^{\zeta}-H^{\gamma}}$ .

Contrary to what we purposed in Scheme 1 where only one transition state is hypothesized for reaction step 2, two transition states in the current reaction process were found. This observation is similar to that in CocE-catalyzed (–)-cocaine hydrolysis where two transition states were characterized in the dissociation of (–)-cocaine benzoyl ester.<sup>32</sup> The two transition states here are denoted by TS2 and TS2'. The intermediate between the two transition states is denoted by INT1'. The QM/MM-optimized geometries of the intermediates and transition states of the current reaction process are given in Figure 3.

In the geometry of INT1 where the serine hydroxyl proton ( $H^{\gamma}$ ) has been transferred to the  $N^{\epsilon}$  atom of His287 in reaction step 1, the distance ( $R_{O^{\gamma}-H^{\gamma}}$ ) between the  $O^{\gamma}$  atom of the Ser117 side chain and the  $H^{\gamma}$  atom of the His287 side chain is 2.02 Å, indicating a strong hydrogen bond of  $N^{\epsilon}-H^{\gamma}\cdots O^{\gamma}$  between the Ser117 and His287 side chains. However, the distance ( $R_{O^{\zeta}-H^{\gamma}}$ ) between  $H^{\gamma}$  and the leaving ester oxygen ( $O^{\zeta}$ ) to which  $H^{\gamma}$  is about to be transferred is 2.67 Å, indicating a very weak hydrogen bond between the  $H^{\gamma}$  and  $O^{\zeta}$  atoms and an environment unsuitable for proton transfer from the  $N^{\epsilon}$  atom of His287 to the leaving ester oxygen ( $O^{\zeta}$ ) atom. In changing from INT1 to INT1', there are two major structural changes. One is the gradual breaking of the covalent bond  $C^{\zeta}-O^{\zeta}$  ( $R_{C^{\zeta}-O^{\zeta}}$  is 1.58 Å in INT1, 1.90 Å in TS2, and 2.73 Å in INT1'). The other is the formation of the hydrogen bond  $N^{\epsilon}-H^{\gamma}\cdots O^{\zeta}$  indicated by the decreasing distance  $R_{O^{\zeta}-H^{\gamma}}$  in going from INT1 to INT1' (2.67 Å in INT1, 2.38 Å in TS2, and 1.62 Å in INT1'). In the meantime, the hydrogen bond  $N^{\epsilon}-H^{\gamma}\cdots O^{\gamma}$  formed between the transferring proton ( $H^{\gamma}$ ) and the  $O^{\gamma}$  atom of Ser117 becomes progressively weaker ( $R_{O^{\gamma}-H^{\gamma}}$  is 2.02 Å in INT1, 2.16 Å in TS2, and 2.68 Å in INT1'), which is reasonable as the transferring proton ( $H^{\gamma}$ ) is about to be transferred to the leaving ester oxygen ( $O^{\zeta}$ ) in the current reaction step.

The major difference between INT1' and TS2' is the position of the transferring proton ( $H^{\gamma}$ ), while the distance  $R_{C^{\zeta}-O^{\zeta}}$  remains unchanged, indicating that the reaction process associated with TS2' is primarily the proton ( $H^{\gamma}$ ) transfer from the  $N^{\epsilon}$  atom of the His287 side chain to the leaving ester oxygen ( $O^{\zeta}$ ) atom ( $R_{O^{\zeta}-H^{\gamma}}$  is 1.62 Å in INT1', 1.54 Å in TS2', and 0.99 Å in INT2;  $R_{N^{\epsilon}-H^{\gamma}}$  is 1.07 Å in INT1', 1.09 Å in TS2', and 1.87 Å in

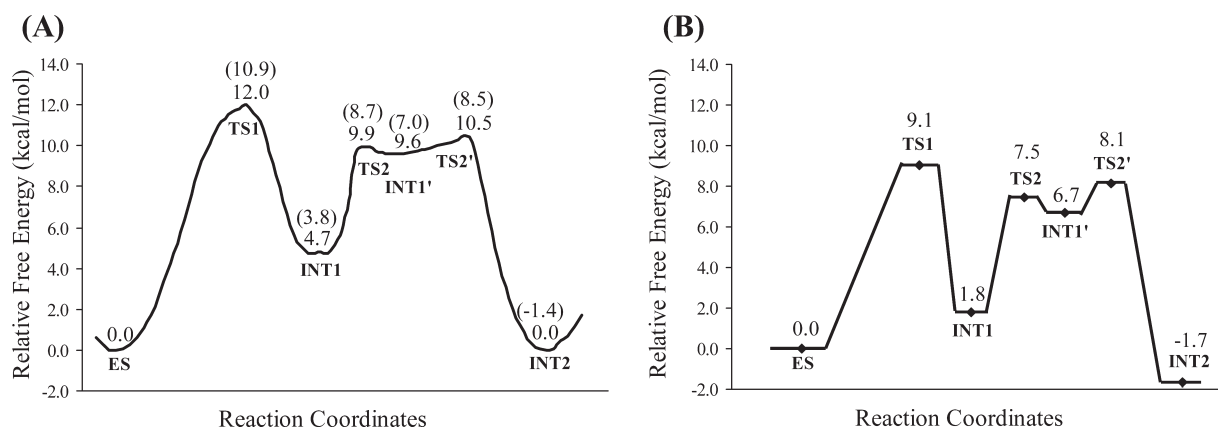


**Figure 4.** (A) Free energy profile determined by the MP2/6-31+G\*:AMBER QM/MM-FE calculations excluding the zero-point and thermal corrections for the QM subsystem. The values in parentheses are relative free energies including zero-point and thermal corrections for the QM subsystem. (B) Relative free energies with both zero-point and thermal corrections for the QM subsystem and electrostatic corrections from counterions.

INT2). Therefore, the proton transfer in the current reaction process proceeds not simultaneously with but only after the breaking of the C–O covalent bond.

**Catalytic Role of the Oxyanion Hole.** It is interesting to know the catalytic role of the oxyanion hole consisting of the backbone amide of Tyr118 and the hydroxyl group of the Tyr44 side chain. On the basis of the QM/MM reaction coordinate calculations, throughout the acylation stage of (+)-cocaine hydrolysis, the carbonyl oxygen ( $O^{\prime}$ ) of (+)-cocaine forms two hydrogen bonds with the oxyanion hole. One is the hydrogen bond of  $O-H^{\prime} \cdots O^{\prime}$  with the hydroxyl hydrogen ( $H^{\prime}$ ) atom of Tyr44 side chain, and the other is the hydrogen bond of  $N-H^{\prime} \cdots O^{\prime}$  with the backbone NH group ( $H^{\prime}$  atom) of Tyr118. As one can see from Figures 2 and 3, the hydrogen bond  $O-H^{\prime} \cdots O^{\prime}$  between the  $O^{\prime}$  atom and Tyr44 hydroxyl is very strong throughout the acylation stage with a distance of  $\sim 1.8$  Å. The other hydrogen bond  $N-H^{\prime} \cdots O^{\prime}$  between the  $O^{\prime}$  atom and Tyr118 backbone NH group is relatively weaker than that with the Tyr44 hydroxyl during the reaction. It is weak in ES with a distance of  $\sim 2.6$  Å and then becomes stronger with a distance of  $\sim 2.1$  Å in the subsequent states of the reaction. Therefore, both hydrogen bonds stabilize the negative charge of the carbonyl oxygen ( $O^{\prime}$ ) developing during the hydrolysis, where the primary contribution to the stabilization comes from Tyr44.

**Energetics and Kinetic Parameters.** Using the QM/MM-optimized geometries at the QM/MM(B3LYP/6-31G\*:AMBER) level, we carried out QM/MM single-point energy calculations at the QM/MM(MP2/6-31+G\*:AMBER) level for each geometry along the minimum-energy path. For each geometry along the minimum-energy path, the ESP charges determined in the QM subsystem of the QM/MM single-point energy calculation were used in subsequent FEP simulations for estimating the free energy changes along the reaction path. Depicted in Figure 4A is the energy profile determined by the QM/MM-FE calculations excluding the zero-point and thermal corrections for the QM subsystem. The values given in parentheses are the corresponding relative free energies with the zero-point and thermal corrections for the QM subsystem. It has been pointed out in our previous study<sup>32</sup> that, although the counterions in the CocE system are not directly involved in the reaction mechanism, the interaction (particularly the electrostatic

**Table 1.** Final Relative Free Energies for CocE-Catalyzed Hydrolyses of (+)- and (–)-Cocaine

reaction stage	geometry	relative free energy (kcal/mol)	
		(–)-cocaine <sup>a</sup>	(+)-cocaine
acylation	ES	0.0	0.0
	TS1	2.3	9.1
	INT1	–5.3	1.8
	TS2	–2.6	7.5
	INT1'	NA <sup>b</sup>	6.7
	TS2'	NA <sup>b</sup>	8.1
deacylation	INT2	–13.1	–1.7
	INT2'	0.0	0.0
	TS3	17.9	17.9
	INT3	14.8	14.8
	TS4	17.5	17.5
	PD	–3.8	–3.8

<sup>a</sup>Data for (–)-cocaine are all from ref 32. <sup>b</sup>NA = not applicable. The energy barrier associated with TS2' on the potential energy surface was too small ( $\sim 0.1$  kcal/mol) for the (–)-cocaine hydrolysis, and the barrier disappeared after the FEP simulation was applied.

interaction) between the QM subsystem and the large number of counterions in the CocE system is significant in determining the free energy barrier of the reaction. Therefore, in the present study, we also estimated the electrostatic interaction between the QM subsystem and counterions, which can be considered as the correction with counterions to the free energies, by following the same computational strategy as in our previous study on the CocE-catalyzed (–)-cocaine hydrolysis where the coordinates of the counterions in 100 snapshots were taken out (one snapshot in each 10 ps) of the MD trajectory.<sup>32</sup> The relative free energies with both zero-point and thermal corrections for the QM subsystem and electrostatic corrections with the counterions are shown in Figure 4B. The calculated final free energy barriers are summarized in Table 1 in comparison with those calculated for CocE-catalyzed hydrolysis of (–)-cocaine.

As shown in Figure 4B, the relative free energy (9.1 kcal/mol) associated with TS1 is slightly higher than those associated with

**Table 2. Kinetic Parameters Determined for CocE-Catalyzed Hydrolyses of (+)- and (-)-Cocaine**

(+) -cocaine		(-) -cocaine	
$K_M$ ( $\mu\text{M}$ )	$k_{\text{cat}}$ ( $\text{min}^{-1}$ )	$K_M$ ( $\mu\text{M}$ )	$k_{\text{cat}}$ ( $\text{min}^{-1}$ )
$15 \pm 4$	$1078 \pm 250$	$13 \pm 3$	$1082 \pm 181$

the remaining two transition states in the acylation stage, namely, TS2 (7.5 kcal/mol) and TS2' (8.1 kcal/mol). Therefore, the rate-determining step of the acylation stage of CocE-catalyzed (+)-cocaine hydrolysis is the first reaction step, i.e., the nucleophilic attack on the  $C^{\zeta}$  atom by the  $O^{\gamma}$  atom of Ser117. As mentioned in the Introduction, CocE-catalyzed hydrolyses of (+)- and (-)-cocaine share the same deacylation stage. Thus, the free energy profiles for the deacylation of both (+)- and (-)-cocaine by CocE are identical. Our previous study<sup>32</sup> has shown that the calculated free energy barrier of deacylation in the CocE-catalyzed (-)-cocaine hydrolysis, which was found to be rate-determining, is  $\sim 17.9$  kcal/mol. Therefore, the free energy barrier for the deacylation of (+)-cocaine should also be  $\sim 17.9$  kcal/mol, and the deacylation is also rate-determining for CocE-catalyzed (+)-cocaine hydrolysis because its energy barrier is much higher than that of the acylation stage (9.1 kcal/mol).

Now that the common deacylation step is rate-determining for both (+)- and (-)-cocaine hydrolyses catalyzed by CocE, these computational results predict that the catalytic rate constant ( $k_{\text{cat}}$ ) of CocE against (+)-cocaine should be the same as that of CocE against (-)-cocaine. The predicted reaction mechanisms and relative catalytic rate constants of CocE against (+)- and (-)-cocaine are remarkably different from those of BChE against (+)- and (-)-cocaine.<sup>22,23</sup> Human BChE-catalyzed hydrolyses of (+)- and (-)-cocaine have different rate-determining steps and considerably different catalytic rate constants, with a difference of 3 orders of magnitude.<sup>23</sup>

Kinetic parameters for CocE-catalyzed hydrolysis of (+)-cocaine are not available in the literature, although kinetic parameters for CocE-catalyzed hydrolysis of (-)-cocaine were determined previously.<sup>14,18</sup> To examine whether the computational prediction is correct, we also carried out experimental kinetic analysis on CocE-catalyzed hydrolyses of (+)- and (-)-cocaine at the same time under the same experimental conditions. The determined kinetic parameters are summarized in Table 2. As shown in Table 2, the  $k_{\text{cat}}$  values for CocE-catalyzed hydrolyses of (+)- and (-)-cocaine were determined to be  $1078 \pm 250$  and  $1082 \pm 181 \text{ min}^{-1}$ , respectively. The two  $k_{\text{cat}}$  values are identical within the experimental fluctuations, which strongly supports the computational prediction that CocE-catalyzed hydrolyses of (+)- and (-)-cocaine have a common rate-determining reaction step. In addition, the determined two  $K_M$  (Michaelis–Menten constant) values are also identical within the experimental fluctuations.

**Implication from the Mechanistic Insights for Design of an Improved Cocaine Esterase.** The mechanistic differences between (+)- and (-)-cocaine hydrolyses catalyzed by CocE and their rate-determining steps are remarkably different from those catalyzed by human BChE. In the (+)- and (-)-cocaine hydrolyses catalyzed by human BChE, the rate-determining step for the (+)-cocaine hydrolysis is different from that for the (-)-cocaine hydrolysis; the rate-determining step for the (-)-cocaine hydrolysis is a reaction step before the deacylation. As a result, (+)-cocaine hydrolysis in human BChE is about 3 orders

of magnitude faster than the corresponding (-)-cocaine hydrolysis in the same enzyme. Thus, computational design of high-activity mutants of human BChE against (-)-cocaine has been focused on the reaction steps before the deacylation. Unlike BChE, the rate-determining steps for CocE-catalyzed hydrolyses of (+)- and (-)-cocaine are a common reaction step (the first step) in the deacylation stage such that the catalytic rate constants for both (+)- and (-)-cocaine hydrolyses are the same. Therefore, computational design of high-activity mutants of CocE against cocaine should be focused on the first reaction step of the deacylation.

The mechanistic differences between CocE-catalyzed (+)- and (-)-cocaine hydrolyses reside in the acylation stage, which is not rate-determining, and, thus, do not seem to provide direct clues to design a CocE mutant with an improved catalytic activity against (-)-cocaine. Nevertheless, the mechanistic differences between CocE-catalyzed (+)- and (-)-cocaine hydrolyses may indirectly provide beneficial clues to design high-activity mutants of CocE against (-)-cocaine. As reported in our previous study,<sup>32</sup> the free energy barriers for the first and second reaction steps in the acylation of (-)-cocaine are  $\sim 2.3$  and  $\sim 2.7$  kcal/mol, respectively. As shown in Figure 4B and Table 1, the free energy barrier for the first reaction step of CocE-catalyzed hydrolysis of (+)-cocaine is  $\sim 9.1$  kcal/mol, much higher than that for the first or second reaction step of the (-)-cocaine hydrolysis. A detailed analysis of the QM/MM-optimized geometries suggests that the significant difference in the free energy barrier for the first reaction step between the (+)- and (-)-cocaine hydrolyses may be attributed to the difference in the hydrogen bonding with the oxyanion hole in the transition state TS1. As discussed above, there are two hydrogen bonds between the carbonyl oxygen ( $O^{\eta}$ ) of the substrate and the oxyanion hole consisting of the hydroxyl group ( $O-H^{\eta}$ ) of the Tyr44 side chain and the backbone NH group ( $H^{\kappa}$  atom) of Tyr118. In the TS1 geometry with (+)-cocaine, as depicted in Figure 2B, the optimized  $H^{\eta} \cdots O^{\eta}$  and  $H^{\kappa} \cdots O^{\eta}$  distances were 1.99 and 2.20 Å, respectively. In the corresponding TS1 geometry with (-)-cocaine, the optimized  $H^{\eta} \cdots O^{\eta}$  and  $H^{\kappa} \cdots O^{\eta}$  distances were 1.75 and 2.25 Å, respectively.<sup>32</sup> The overall hydrogen bonding of the oxyanion hole with (-)-cocaine should be significantly stronger than that with (+)-cocaine. The possible effect of the hydrogen bonding on the TS1 stabilization may provide some indirect clues in rational design of high-activity mutants of CocE against cocaine, because the two similar hydrogen bonds also exist in the transition state (denoted by TS3) for the rate-determining step, deacylation.<sup>32</sup> Apparently, certain amino acid mutations capable of enhancing the overall hydrogen bonding with the oxyanion hole in the TS3 structure could decrease the energy barrier for the rate-determining step and thus improve the catalytic activity of the enzyme against cocaine.

## CONCLUSION

Results from the first-principle QM/MM-FE calculations demonstrate that the acylation stage of CocE-catalyzed hydrolysis of (+)-cocaine is initiated by the attack of the hydroxyl oxygen ( $O^{\gamma}$ ) of Ser117 on the carbonyl carbon ( $C^{\zeta}$ ) of (+)-cocaine benzoyl ester. This process is facilitated by His287 through proton ( $H^{\gamma}$ ) transfer from the Ser117 hydroxyl to the  $N^{\epsilon}$  atom of the His287 side chain, which increases the nucleophilicity of the Ser117 hydroxyl. His287 is in turn stabilized by the formation of another hydrogen bond between the His287

and Asp259 side chains. The Ser117 nucleophile attacks the electron-deficient C<sup>ε</sup> atom of (+)-cocaine benzoyl ester, forming a tetrahedral intermediate in which the carbonyl oxygen (O<sup>n</sup>) of (+)-cocaine with developing negative charge is stabilized by two tyrosine residues (Tyr44 and Tyr118) in the oxyanion hole. Then His287 transfers a proton (H<sup>+</sup>) to the ester oxygen (O<sup>ε</sup>) of the leaving ecgonine group, completing the acylation stage.

The QM/MM-optimized geometries indicate that the oxyanion hole stabilizes the negative charge of the (+)-cocaine carbonyl oxygen (O<sup>n</sup>) developing during the hydrolysis by providing two hydrogen bonds with Tyr44 and Tyr118. The hydrogen bond with Tyr44 is particularly strong and is the primary factor stabilizing the carbonyl oxygen (O<sup>n</sup>) of (+)-cocaine benzoyl ester.

The highest energy barrier calculated for the acylation of (+)-cocaine is ~9.1 kcal/mol, associated with the first reaction step of acylation. The calculated energy barrier of ~9.1 kcal/mol is much lower than the highest energy barrier for the deacylation (~17.9 kcal/mol, associated with the first reaction step of deacylation). Therefore, the deacylation of (+)-cocaine, which is identical to that of (–)-cocaine, is rate-determining, revealing that CocE-catalyzed hydrolyses of (+)- and (–)-cocaine have a common rate-determining step. All of these results predict that the catalytic rate constant ( $k_{\text{cat}}$ ) of CocE against (+)-cocaine should be the same as that of CocE against (–)-cocaine, in contrast with the remarkable difference between human BChE-catalyzed hydrolyses of (+)- and (–)-cocaine. The computational prediction has been confirmed by performing experimental kinetic analysis on CocE-catalyzed hydrolysis of (+)-cocaine, for the first time, in comparison with CocE-catalyzed hydrolysis of (–)-cocaine.

The determined common rate-determining reaction step and detailed mechanistic differences in the acylation between CocE-catalyzed hydrolyses of (+)- and (–)-cocaine provide a valuable mechanistic base for future rational design of CocE mutants with an improved catalytic activity against cocaine. In particular, the common rate-determining reaction step indicates that rational design of a high-activity mutant of CocE should be focused on stabilization of the transition-state structure (TS3) for the first reaction step of the deacylation. The mutation-caused stabilization of the transition state for the rate-determining reaction step could lead to a decrease in the overall energy barrier and, thus, an increase in the catalytic rate constant.

## AUTHOR INFORMATION

### Corresponding Author

\*Phone: (859) 323-3943. Fax: (859) 323-3575. E-mail: zhan@uky.edu.

### Author Contributions

<sup>†</sup>These authors contributed equally to this work.

## ACKNOWLEDGMENT

This work was supported in part by the National Institutes of Health (Grants R01 DA025100, R01 DA021416, and R01 DA013930). The entire work was performed at the University of Kentucky. X.Z. worked in C.-G.Z.'s laboratory for this project at the University of Kentucky as an exchange graduate student from Central China Normal University. We thank Drs. Roger K. Sunahara and Diwahar L. Narasimhan at the University of

Michigan Medical School for providing the cDNA samples. We also acknowledge the Center for Computational Sciences at the University of Kentucky for supercomputing time on the IBM X-series cluster with 340 nodes or 1360 processors.

## REFERENCES

- (1) Mendelson, J. H.; Mello, N. K. *N. Engl. J. Med.* **1996**, *334* (15), 965–972.
- (2) Paula, S.; Tabet, M. R.; Farr, C. D.; Norman, A. B.; Ball, W. J. *J. Med. Chem.* **2003**, *47* (1), 133–142.
- (3) Singh, S. *Chem. Rev.* **2000**, *100* (3), 925–1024.
- (4) Substance Abuse and Mental Health Services Administration. *Drug Abuse Warning Network, 2004: National Estimates of Drug-Related Emergency Department Visits*; DAWN Series D-28; DHHS Publication No. SMA 06-4143; Office of Applied Studies, Department of Health & Human Services: Rockville, MD, 2006.
- (5) Sparenborg, S.; Vocci, F.; Zukin, S. *Drug Alcohol Depend.* **1997**, *48* (3), 149–51.
- (6) Gorelick, D. A. *Drug Alcohol Depend.* **1997**, *48* (3), 159–65.
- (7) Gorelick, D. A.; Gardner, E. L.; Xi, Z. X. *Drugs* **2004**, *64* (14), 1547–73.
- (8) Dickerson, T. J.; Janda, K. D. Recent Advances for the Treatment of Cocaine Abuse: Central Nervous System Immunopharmacotherapy. In *Drug Addiction*; Rapaka, R. S., Sadée, W., Eds; Springer: New York, 2008; pp 217–229.
- (9) Gao, D.; Cho, H.; Yang, W.; Pan, Y.; Yang, G.; Tai, H.-H.; Zhan, C.-G. *Angew. Chem., Int. Ed.* **2006**, *45* (4), 653–657.
- (10) Vocci, F. J.; Aciri, J.; Elkashef, A. *Am. J. Psychiatry* **2005**, *162* (8), 1432–1440.
- (11) Zheng, F.; Yang, W.; Ko, M.-C.; Liu, J.; Cho, H.; Gao, D.; Tong, M.; Tai, H.-H.; Woods, J. H.; Zhan, C.-G. *J. Am. Chem. Soc.* **2008**, *130* (36), 12148–12155.
- (12) Pan, Y.; Gao, D.; Yang, W.; Cho, H.; Yang, G.; Tai, H.-H.; Zhan, C.-G. *Proc. Natl. Acad. Sci. U.S.A.* **2005**, *102* (46), 16656–16661.
- (13) Bresler, M. M.; Rosser, S. J.; Basran, A.; Bruce, N. C. *Appl. Environ. Microbiol.* **2000**, *66* (3), 904–908.
- (14) Larsen, N. A.; Turner, J. M.; Stevens, J.; Rosser, S. J.; Basran, A.; Lerner, R. A.; Bruce, N. C.; Wilson, I. A. *Nat. Struct. Mol. Biol.* **2002**, *9* (1), 17–21.
- (15) Cooper, Z. D.; Narasimhan, D.; Sunahara, R. K.; Mierzejewski, P.; Jutkiewicz, E. M.; Larsen, N. A.; Wilson, I. A.; Landry, D. W.; Woods, J. H. *Mol. Pharmacol.* **2006**, *70* (6), 1885–1891.
- (16) Ko, M.-C.; Bowen, L. D.; Narasimhan, D.; Berlin, A. A.; Lukacs, N. W.; Sunahara, R. K.; Cooper, Z. D.; Woods, J. H. *J. Pharmacol. Exp. Ther.* **2007**, *320* (2), 926–933.
- (17) Emily, M. J.; Michelle, G. B.; Ziva, D. C.; Diwahar, N.; Roger, K. S.; James, H. W. *Ann. Emerg. Med.* **2008**, *54*, 409–420.
- (18) Gao, D.; Narasimhan, D. L.; Macdonald, J.; Brim, R.; Ko, M.-C.; Landry, D. W.; Woods, J. H.; Sunahara, R. K.; Zhan, C.-G. *Mol. Pharmacol.* **2009**, *75* (2), 318–323.
- (19) Brim, R. L.; Nance, M. R.; Youngstrom, D. W.; Narasimhan, D.; Zhan, C.-G.; Tesmer, J. J. G.; Sunahara, R. K.; Woods, J. H. *Mol. Pharmacol.* **2010**, *77* (4), 593–600.
- (20) Collins, G. T.; Brim, R. L.; Narasimhan, D.; Ko, M. C.; Sunahara, R. K.; Zhan, C.-G.; Woods, J. H. *J. Pharmacol. Exp. Ther.* **2009**, *331* (2), 445–455.
- (21) Narasimhan, D.; Nance, M. R.; Gao, D.; Ko, M.-C.; Macdonald, J.; Tamburi, P.; Yoon, D.; Landry, D. M.; Woods, J. H.; Zhan, C.-G.; Tesmer, J. J. G.; Sunahara, R. K. *Protein Eng. Des. Sel.* **2010**, *23*, 537–547.
- (22) Zhan, C.-G.; Gao, D. Q. *Biophys. J.* **2005**, *89* (6), 3863–3872.
- (23) Zhan, C.-G.; Zheng, F.; Landry, D. W. *J. Am. Chem. Soc.* **2003**, *125* (9), 2462–74.
- (24) Sun, H.; Pang, Y.-P.; Lockridge, O.; Brimijoin, S. *Mol. Pharmacol.* **2002**, *62* (2), 220–224.
- (25) Gao, Y.; Atanasova, E.; Sui, N.; Pancook, J. D.; Watkins, J. D.; Brimijoin, S. *Mol. Pharmacol.* **2005**, *67* (1), 204–211.

- (26) Gao, D. Q.; Zhan, C.-G. *J. Phys. Chem. B* **2005**, *109* (48), 23070–23076.
- (27) Hamza, A.; Cho, H.; Tai, H.-H.; Zhan, C.-G. *J. Phys. Chem. B* **2005**, *109* (10), 4776–4782.
- (28) Sun, H.; El Yazal, J.; Lockridge, O.; Schopfer, L. M.; Brimijoin, S.; Pang, Y. P. *J. Biol. Chem.* **2001**, *276* (12), 9330–9336.
- (29) Sun, H.; Shen, M. L.; Pang, Y. P.; Lockridge, O.; Brimijoin, S. *J. Pharmacol. Exp. Ther.* **2002**, *302* (2), 710–716.
- (30) Yang, W. C.; Xue, L.; Fang, L.; Chen, X.; Zhan, C.-G. *Chem.-Biol. Interact.* **2010**, *187* (1–3), 148–152.
- (31) Zheng, F.; Yang, W. C.; Xue, L.; Hou, S. R.; Liu, J. J.; Zhan, C.-G. *Biochemistry* **2010**, *49* (42), 9113–9119.
- (32) Liu, J.; Hamza, A.; Zhan, C.-G. *J. Am. Chem. Soc.* **2009**, *131* (33), 11964–75.
- (33) Turner, J. M.; Larsen, N. A.; Basran, A.; Barbas, C. F.; Bruce, N. C.; Wilson, I. A.; Lerner, R. A. *Biochemistry* **2002**, *41* (41), 12297–12307.
- (34) Zheng, F.; Zhan, C.-G. *Org. Biomol. Chem.* **2008**, *6* (5), 836–843.
- (35) Pan, Y. M.; Gao, D. Q.; Yang, W. C.; Cho, H.; Zhan, C.-G. *J. Am. Chem. Soc.* **2007**, *129* (44), 13537–13543.
- (36) Gao, D. Q.; Zhan, C.-G. *Proteins* **2006**, *62* (1), 99–110.
- (37) Zhang, Y. K. *J. Chem. Phys.* **2005**, *122* (2), 024114.
- (38) Zhang, Y. K.; Lee, T. S.; Yang, W. T. *J. Chem. Phys.* **1999**, *110* (1), 46–54.
- (39) Zhang, Y. K.; Liu, H. Y.; Yang, W. T. *J. Chem. Phys.* **2000**, *112* (8), 3483–3492.
- (40) Zhang, Y. K. *Theor. Chem. Acc.* **2006**, *116* (1–3), 43–50.
- (41) Hu, P.; Zhang, Y. K. *J. Am. Chem. Soc.* **2006**, *128* (4), 1272–1278.
- (42) Liu, H.; Zhang, Y.; Yang, W. *J. Am. Chem. Soc.* **2000**, *122* (28), 6560–6570.
- (43) Zhang, Y.; Kua, J.; McCammon, J. A. *J. Am. Chem. Soc.* **2002**, *124* (35), 10572–10577.
- (44) Cisneros, G. A.; Liu, H.; Zhang, Y.; Yang, W. *J. Am. Chem. Soc.* **2003**, *125* (34), 10384–10393.
- (45) Zhang, Y.; Kua, J.; McCammon, J. A. *J. Phys. Chem. B* **2003**, *107* (18), 4459–4463.
- (46) Cheng, Y.; Zhang, Y.; McCammon, J. A. *J. Am. Chem. Soc.* **2005**, *127* (5), 1553–1562.
- (47) Corminboeuf, C.; Hu, P.; Tuckerman, M. E.; Zhang, Y. *J. Am. Chem. Soc.* **2006**, *128* (14), 4530–4531.
- (48) Wang, L.; Yu, X.; Hu, P.; Broyde, S.; Zhang, Y. *J. Am. Chem. Soc.* **2007**, *129* (15), 4731–4737.
- (49) Wang, S.; Hu, P.; Zhang, Y. *J. Phys. Chem. B* **2007**, *111* (14), 3758–3764.
- (50) Xiao, C.; Zhang, Y. *J. Phys. Chem. B* **2007**, *111* (22), 6229–6235.
- (51) Hu, P.; Wang, S.; Zhang, Y. *J. Am. Chem. Soc.* **2008**, *130* (12), 3806–3813.
- (52) Cheng, Y.; Zhang, Y.; McCammon, J. A. *Protein Sci.* **2006**, *15* (4), 672–683.
- (53) Case, D. A.; Darden, T. A.; T.E. Cheatham, I.; Simmerling, C. L.; Wang, J.; Duke, R. E.; Luo, R.; Merz, K. M.; Wang, B.; Pearlman, D. A.; Crowley, M.; Brozell, S.; Tsui, V.; Gohlke, H.; Mongan, J.; Hornak, V.; Cui, G.; Beroza, P.; Schafmeister, C.; Caldwell, J. W.; Ross, W. S.; Kollman, P. A. *AMBER 8*; University of California: San Francisco, 2004.
- (54) Frisch, M. J.; Trucks, G. W.; Schlegel, H. B.; Scuseria, G. E.; Robb, M. A.; Cheeseman, J. R.; Montgomery, J. A.; Vreven, T.; Kudin, K. N.; Burant, J. C.; Millam, J. M.; Iyengar, S. S.; Tomasi, J.; Barone, V.; Mennucci, B.; Cossi, M.; Scalmani, G.; Rega, N.; Petersson, G. A.; Nakatsuji, H.; Hada, M.; Ehara, M.; Toyota, K.; Fukuda, R.; Hasegawa, J.; Ishida, M.; Nakajima, T.; Honda, Y.; Kitao, O.; Nakai, H.; Klene, M.; Li, X.; Knox, J. E.; Hratchian, H. P.; Cross, J. B.; Bakken, V.; Adamo, C.; Jaramillo, J.; Gomperts, R.; Stratmann, R. E.; Yazyev, O.; Austin, A. J.; Cammi, R.; Pomelli, C.; Ochterski, J. W.; Ayala, P. Y.; Morokuma, K.; Voth, G. A.; Salvador, P.; Dannenberg, J. J.; Zakrzewski, V. G.; Dapprich, S.; Daniels, A. D.; Strain, M. C.; Farkas, O.; Malick, D. K.; Rabuck, A. D.;